BJ www.biochemj.org

BJ Structure

Biochem. J. (2011) **435**, 577–587 (Printed in Great Britain) doi:10.1042/BJ20101548

online data

Autotransporter passenger domain secretion requires a hydrophobic cavity at the extracellular entrance of the β-domain pore

Yujia ZHAI*, Kai ZHANG*[1], Yanwu HUO*[1], Yanshi ZHU†, Qiangjun ZHOU*, Jiuwei LU*, Isobel BLACK†, Xiaoyun PANG*, Aleksander W. ROSZAK†, Xujia ZHANG*, Neil W. ISAACS† and Fei SUN*[2]

*National Laboratory of Biomacromolecules, Institute of Biophysics, Chinese Academy of Sciences, Beijing 100101, China, and †Department of Chemistry and WestChem, University of Glasgow, Glasgow G12 8QQ, U.K.

Whooping cough (pertussis) is a highly contagious acute respiratory illness of humans caused by the Gram-negative bacterial pathogen *Bordetella pertussis*. The AT (autotransporter) BrkA (*Bordetella* serum-resistance killing protein A) is an important *B. pertussis* virulence factor that confers serum resistance and mediates adherence. In the present study, we have solved the crystal structure of the BrkA β-domain at 3 Å (1 Å = 0.1 nm) resolution. Special features are a hairpin-like structure formed by the external loop L4, which is observed fortuitously sitting inside the pore of the crystallographic adjacent β-domain, and a previously undiscovered hydrophobic cavity formed by patches on loop L4 and β-strands S5 and S6. This adopts a ubiquitous structure characteristic of all AT β-domains. Mutagenesis studies have demonstrated that the hairpin-like structure and hydrophobic cavity are crucial for BrkA passenger domain (virulence effector) translocation. This structure helps in understanding the molecular mechanism of AT assembly and secretion and provides a potential target for anti-pertussis drug design.

Key words: autotransporter, *Bordetella pertussis*, membrane protein, outer membrane translocation, passenger domain secretion, trypsin-accessibility assay.

INTRODUCTION

Whooping cough (pertussis) is a highly contagious acute respiratory illness of humans caused by the Gram-negative bacterial pathogen *Bordetella pertussis*. Although it was long considered a childhood illness, in reality it can affect all age groups. Despite global childhood immunization, the disease remains fifth among vaccine-preventable death aetiologies in children under 5 years of age [1]. Worldwide, it is estimated that approximately 20–40 million cases occur every year, with 200 000–400 000 childhood deaths [2]. Although ~90 % of the deaths occur in the developing world, there has been an increasing trend in reported pertussis infections in countries with high vaccination coverage, especially in young infants, adolescents and adults [3]. Research efforts are thus being directed at reinforcing existing vaccination strategies and finding new preventive drugs to combat *B. pertussis* [4].

BrkA (*Bordetella* serum-resistance killing protein A) is an important *B. pertussis* virulence factor that confers serum resistance and mediates adherence [5]. BrkA mutants of *B. pertussis* have been shown to be severely defective in their ability to colonize mice and to cause lethal infection in the infant mouse model [5–7]. Recent studies have shown that the recombinant BrkA protein is a promising candidate antigen to improve existing Pa (acellular pertussis) vaccines in humans [8].

BrkA is expressed as a 103 kDa precursor (preBrkA) that is processed during secretion to a 42-amino-acid signal peptide, a 73 kDa passenger domain and a 30 kDa β-domain [5,9–11]. The translated nascent preBrkA is targeted to and translocated across the IM (inner membrane) via a classical Sec-dependent process initiated by the signal peptide [12–14]. After translocation across the IM, the signal peptide is cleaved, yielding the mature precursor (proBrkA) in the periplasm. After the β-domain of proBrkA integrates into the OM (outer membrane), the passenger domain is translocated across the OM and self-cleaved at a site between Asn^{731} and Ala^{732} by an unusual catalytic dyad formed by the cyclization of asparagine [15]. After translocation across the OM, the passenger domain remains tightly associated with the bacterial surface [16]. The β-domain of BrkA shows a pore-forming ability in black lipid bilayer experiments and has 55 % sequence identity with the β-domain of pertactin, another highly immunogenic virulence factor of *B. pertussis* [10].

BrkA belongs to the AT (autotransporter) superfamily whose members are often virulence proteins secreted by Gram-negative bacteria. All ATs contain an N-terminal cleavable signal peptide, a functional passenger domain and a C-terminal β-domain [17,18]. Although the size of the passenger domains is highly variable and often exceeds 100 kDa, all available evidence indicates that the passenger domains of classical ATs adopt a β-helix structure [19–23]. The β-domains of classical ATs are relatively uniform in size (~300 amino acids) and essential for passenger domain translocation across the OM. The crystal structures of the β-domains of NalP and EspP, two classical ATs from *Neisseria meningitidis* and *Escherichia coli* strain O157:H7 respectively and

Abbreviations used: AT, autotransporter; BCA, bicinchoninic acid; BrkA, *Bordetella* serum-resistance killing protein A; BrkAβ, BrkA β-domain; C_8E_4, tetra(ethylene glycol) (mono-octyl)ether; D, pseudo-dimer; ESRF, European Synchrotron Radiation Facility; FBS, fetal bovine serum; IM, inner membrane; IPTG, isopropyl β-D-thiogalactopyranoside; L, loop; LDAO, *N*,*N*-dimethyldodecylamine-*N*-oxide; LS, light scattering; M, molecule; MR, molecular replacement; NCS, non-crystallographic symmetry; OM, outer membrane; Omp85, outer membrane protein 85; PEG, poly(ethylene glycol); RI, refractive index; RMSD, root mean square deviation; S, β-strand; SEC, size-exclusion chromatography; SEC-MALS, SEC with multi-angle light-scattering detection; SNR, signal-to-noise ratio; T, periplasmic turn.

[1] These authors contributed equally to this work.

[2] To whom correspondence should be addressed (email feisun@ibp.ac.cn).

The crystal structure co-ordinates of BrkA β-domain have been deposited in the PDB with accession number 3QQ2.

EstA, a full-length AT esterase from *Pseudomonas aeruginosa* have been reported [24–26]. All of these AT structures have a common 12-stranded β-barrel domain with a N-terminal α-helix located in the hydrophilic central pore. There are also several disease-related virulence passenger domains whose crystal structures have been determined [19,20,23,27]. However, the mechanism used to translocate the passenger domains across the OM still remains unclear. Four major models have been proposed for the AT passenger domain translocation mechanism: (i) the threading model, (ii) the hairpin model, (iii) the multimer model, and (iv) the Omp85 (outer membrane protein 85)-mediated model [28]. The threading model, whereby translocation is initiated by the insertion of the N-terminus of the passenger domain into the β-domain pore, has been questioned, as there are no specific N-terminal motifs found to initiate the insertion [29]. The hairpin model involves the formation of a hairpin-like structure at the C-terminus of the passenger domain followed by a sliding of the proximal polypeptide through the pore [18,30]. The multimer model argues that the passenger domain (which may be folded at least partially in the periplasm) is transported across the OM through a large common channel formed by an oligomerization of at least six β-domains [31]. In the Omp85-mediated model, exogenous factors such as the Omp85-containing OM complex interact with the β-domain of AT and drive the passenger domain translocation [28].

A thorough understanding of how virulence factors are secreted and what elements of the β-domain are important for passenger domain translocation is of great importance for drug development, as this domain is a potential target for the design of compounds to inhibit the translocation of virulence factors across the OM. In the present study, we solved the crystal structure of the BrkA β-domain (BrkAβ) at a resolution of 3 Å (1 Å = 0.1 nm). Structural analysis and mutagenesis studies revealed a hydrophobic cavity, at the extracellular entrance of the β-domain, which is crucial for passenger domain translocation. Our study gives new insights into the molecular mechanism of AT secretion and provides a potential target for anti-pertussis drug design.

EXPERIMENTAL

Protein expression, refolding and purification

The DNA fragment encoding BrkAβ (residues Ala^{728}–Phe^{1010}) was constructed in expression vector pET11a (Novagen). The protein was overexpressed as inclusion bodies in *E. coli* strain BL21(DE3). The cells were washed in buffer A, containing 50 mM Tris/HCl (pH 8.0), 200 mM NaCl and 10 mM benzamidine, and lysed by sonication in buffer A containing 1 % (v/v) Triton X-100. After centrifugation at 20 000 ***g*** for 30 min, the pellet was washed with buffer A to remove the detergent. Inclusion bodies containing BrkAβ were solubilized in buffer A with the addition of 8 M urea. Refolding was initiated by rapid 10-fold dilution of the urea-solubilized protein into buffer A with 0.5 % LDAO (*N*,*N*-dimethyldodecylamine-*N*-oxide) added. Refolding was carried out for 72 h at 37 °C. The protein was subsequently dialysed against buffer C, containing 25 mM Tris/HCl (pH 8.0), 100 mM NaCl, and 0.06 % LDAO. sulfopropyl-Sepharose chromatography was performed on an ÄKTA prime instrument (GE Healthcare) in buffer C, and a linear gradient up to 500 mM NaCl was used to elute the target protein. BrkAβ was purified further by ion-exchange chromatography with a Resource S column (1 ml; GE Healthcare) that was equilibrated in 20 mM Hepes (pH 7.5) and 0.06 % LDAO on a Biologic Duoflow system (Bio-Rad Laboratories). Applying a very small elution gradient of NaCl from 100 mM to 250 mM, two peaks were eluted and fractionated. Fractions in the first peak were collected and purified further by applying to a Mono S column (1 ml; GE Healthcare), during which the detergent LDAO was exchanged to 0.6 % C_8E_4 [tetra(ethylene glycol) (monooctyl)ether]. The purified BrkAβ protein was then concentrated and used for crystallization.

SEC-MALS (size-exclusion chromatography with multi-angle light-scattering detection)

The instrumental set up used for SEC-MALS experiments consisted of an Agilent Technologies 1100 HPLC system connected in series with a DAWN® HELEOS™ II light-scattering detector (Wyatt Technology) and an Optilab rEX interferometric refractometer detector (Wyatt Technology). The purified BrkAβ protein was diluted to a concentration of ~5 mg/ml in SEC (size-exclusion chromatography) buffer 1 (20 mM Hepes, pH 7.5, 150 mM NaCl and 0.06 % LDAO). Analytical SEC was performed at 16 °C using a Shodex Protein 803 KW column (Shoko America) equilibrated with SEC buffer 1. A 50 μl volume of diluted protein was injected into the column and eluted at a flow rate of 0.5 ml/min. The column effluent was monitored in-line with three detectors that simultaneously monitored UV absorption, LS (light scattering) and the RI (refractive index). Detector outputs were digitized and acquired by a computer running ASTRA software (Wyatt Technology). The resulting three chromatograms were aligned after correcting the inter-detector volume delays between the UV absorption and LS and between the RI and LS detectors. The oligomeric molecular mass of BrkAβ at the eluted peak was calculated using ASTRA software as described previously [32,33]. Two further runs with selected detergents were performed in SEC buffer 2 (20 mM Hepes, pH 7.5, 150 mM NaCl and 0.02 % dodecyl maltoside) and SEC buffer 3 (20 mM Hepes, pH 7.5, 150 mM NaCl and 0.6 % C_8E_4) respectively.

Crystallization and heavy-atom soaking

The solution concentration of BrkAβ was assayed by the BCA (bicinchoninic acid) method then diluted to ~25 mg/ml with 20 mM Hepes (pH 7.5) and 0.6 % C_8E_4. A second detergent, DHDM (2,6-dimethyl-4-heptyl-β-D-maltopyranoside), was added into the protein solution with a final concentration of 55 mM. Crystals were grown at 18 °C by the hanging-drop vapour-diffusion method. The best crystals were grown from a mixture of 1 μl of protein solution and 1 μl of mother liquor {100 mM Tris, pH 8.5, 17 % PEG [poly(ethylene glycol)] 2000, 200 mM LiCl and 15 mM spermidine} over a 200 μl reservoir solution (100 mM Tris/HCl pH 8.5, 28 % PEG2000 and 200 mM LiCl). To screen for heavy-atom compounds bound to BrkAβ, a native gel-shift assay was performed. The heavy-atom derivatives were prepared by adding $K_2Pt(NO_2)_4$ directly into the crystallization drop with a final concentration of 5 mM and soaking for 3 weeks. Crystals were collected and frozen directly in liquid nitrogen without additional cryoprotectant. Heavy-atom soaking improved the diffraction quality with smaller mosaicity and better resolution from 3.5 to 3.0 Å at the synchrotron, although no heavy atoms were found in the final electron density. We speculate that it was the dehydration effect, rather than heavy-atom binding, that improved the crystal quality.

Data collection and structure determination

Several native datasets were collected from the preliminary crystals at the ESRF (European Synchrotron Radiation Facility),

Table 1 Data collection and refinement statistics

The corresponding parameters for the highest-resolution shell are shown in parentheses. $R_{merge} = \Sigma_h \Sigma_i |I_{ih} - <I_h>| / \Sigma_h \Sigma_i <I_h>$, where $<I_h>$ is the mean intensity of the reflection h. $R_{work} = \Sigma(||F_o| - |F_c||)/\Sigma|F_o|$; $R_{free} = R_{factor}$ for a selected subset (5 %) of the reflections that was not included in previous refinement calculations.

Parameter	Value
Cell dimensions	
Space group	$C222_1$
a, b, c (Å)	60.5, 122.4, 406.6
α, β, γ (°)	90, 90, 90
Data collection	
Wavelength (Å)	1.07190
Resolution (Å)	15.0–3.0 (3.1–3.0)
R_{merge}	0.145 (0.315)
I/σ	35.4 (3.3)
Completeness (%)	96.5 (75.0)
Redundancy	8.4 (5.1)
Matthews coefficient (Å^3/Da)	4.04
Wilson B-factor (Å^2)	97.3
Refinement	
Resolution (Å)	15.0–3.0
Number of reflections	30957
R_{work}/R_{free} (%)	26.6/32.4
Number of atoms	
Protein	5781
B-factors (Å^2)	93.1
RMSD	
Bond lengths (Å)	0.012
Bond angles (°)	1.588

Grenoble, France, but the crystals showed twinning and attempts to phase the data by MR (molecular replacement) failed. $K_2Pt(NO_2)_4$-soaked crystals were subsequently used to collect SAD (single anomalous diffraction) data at 100 K at beamline BL17U, SSRF (Shanghai Synchrotron Radiation Facility), Shanghai, China. The wavelength is 1.07190 Å at the platinum absorption peak. To avoid the CCD (charge-coupled device) detector saturation at low-resolution diffraction while using strong beam intensity and recording high SNR (signal-to-noise ratio) data for high-resolution diffraction, two separate datasets were collected. One dataset was collected with a high beam attenuation (0.6 mm thickness) and a large beamstop-to-crystal distance to ensure accurate intensity detection at low resolution (to 45 Å). The second dataset was collected with small beam attenuation (0.4 mm thickness) and a short beamstop-to-crystal distance to stop diffraction lower than 15 Å and increase the SNR for high-resolution diffraction. As a membrane protein crystal, the solvent content of BrkAβ crystal is very high: 69.6 % with the Matthews coefficient 4.04 Å^3/Da (Table 1). As a result, the BrkAβ crystals were more sensitive to radiation damage and the total exposure time was carefully estimated using RADDOSE [34] to avoid severe radiation damage and crystal decay. Owing to one long unit cell axis of 406.6 Å, the orientation of the crystal was carefully manipulated to minimize the number of overlapping diffraction spots. All datasets were processed and merged using HKL2000 [35].

Although an anomalous signal was detected from the diffraction data, phasing was unsuccessful, owing to the low occupancy and high mobility of the heavy atoms. Eventually, the crystal structure of BrkAβ was determined by MR. The starting model used was the crystal structure of EspP (PDB code 2QOM) [25] with side chains truncated to alanine or glycine, except where sequence alignment suggested identity. The Matthews coefficient calculation suggested that there are possibly three or four molecules in one asymmetric unit with solvent content of 69.6 and 59.5 % respectively. A self-rotation function computed by MOLREP [36] gave no significant peak for either three-fold or four-fold non-crystallographic symmetry. The best solution obtained from an MR computation, using MOLREP to search for four molecules in the asymmetric unit, exhibited severe steric clashes, invalidating the possibility of four molecules in one asymmetric unit. The molecule causing severe clashes was deleted and the remaining three (named as M1, M2 and M3; see Figure 2) used for further phasing. (Interestingly, the relative positions and orientations of these could not be obtained if MOLREP was used to search for three molecules in an asymmetric unit.)

Although the initial electron-density map had a good appearance in a number of regions, further density modification and phase refinement did not give significant improvement or decreased R-factors (R_{work}/R_{free} = 42.9/49.1). An examination of the map showed good density for M2 and M3, but relatively poor density for M1. Molecules M2 and M3 had a shoulder-to-shoulder packing similar to that of EspP, and molecule M3 and its crystallographic symmetric neighbour M4 (see Figure 2) were packed head-to-head. Similar head-to-head packing between M1 and M2 could be obtained by rotating molecule M1 by 180°, exchanging the extracellular and intracellular ends. Working on the hypothesis that, in Nature, the crystal packing should the simplest available, we inverted the orientation of molecule M1 and used this modified MR solution for further phasing. Rigid-body refinement of this model decreased the R-factors significantly (R_{work}/R_{free} 35.6/40.5), proving our hypothesis. The density map was dramatically improved further by imposing the NCS (non-crystallographic symmetry) averaging combined with phase extension from 8.0 to 3.0 Å. The averaged density map showed very good connectivity, and most residues could be traced and docked into the sequence. Conserved residues between EspP and BrkAβ and large residues such as tryptophan and tyrosine were assigned and used as a reference to locate other residues during model building. Cycles of structure refinement were performed using CNS [37] with the NCS restriction. A negative B-factor (-50 Å^2) was applied to sharpen the $2F_o - F_c$ map that was used to rebuild the model and correct some errors. After further model building and refinement by CNS, Refmac [38] was used for a final TLS (Translation Liberation Screw-motion) refinement without the NCS restriction. The crystal structure of BrkAβ was finally refined to 3.0 Å with R_{work} of 26.6 %, R_{free} of 32.4 % and an overall FOM (figure of merit) of 0.78. The final electron-density map has good consistency with the structural model (see Supplementary Figure S1 at http://www.BiochemJ.org/bj/435/bj4350577add.htm). The average B-factor of the final refined structure is 93.1 Å^2, close to the calculated Wilson B-factor of 97.3 Å^2. The high B-factor is thought to be due to the high solvent content and radiation damage. No water molecules were added into the model owing to the edge resolution of 3.0 Å. There is an elongated stretch of electron density present in the central pore of the structure, which is too smeared to trace any residues (see Supplementary Figure S2 at http://www.BiochemJ.org/bj/435/bj4350577add.htm). The statistics for data collection, processing and structure refinement are summarized in Table 1.

Mutagenesis, trypsin accessibility assay and Western blot analysis

The DNA fragments of BrkAΔ-PC and its 12 mutants (BrkAΔ-1–12) were cloned (see Figure 4A and Table 2) by the overlapping PCR method from the plasmid pD06935 containing the full-length BrkA [9] and inserted into the vector pEXS-DH [32].

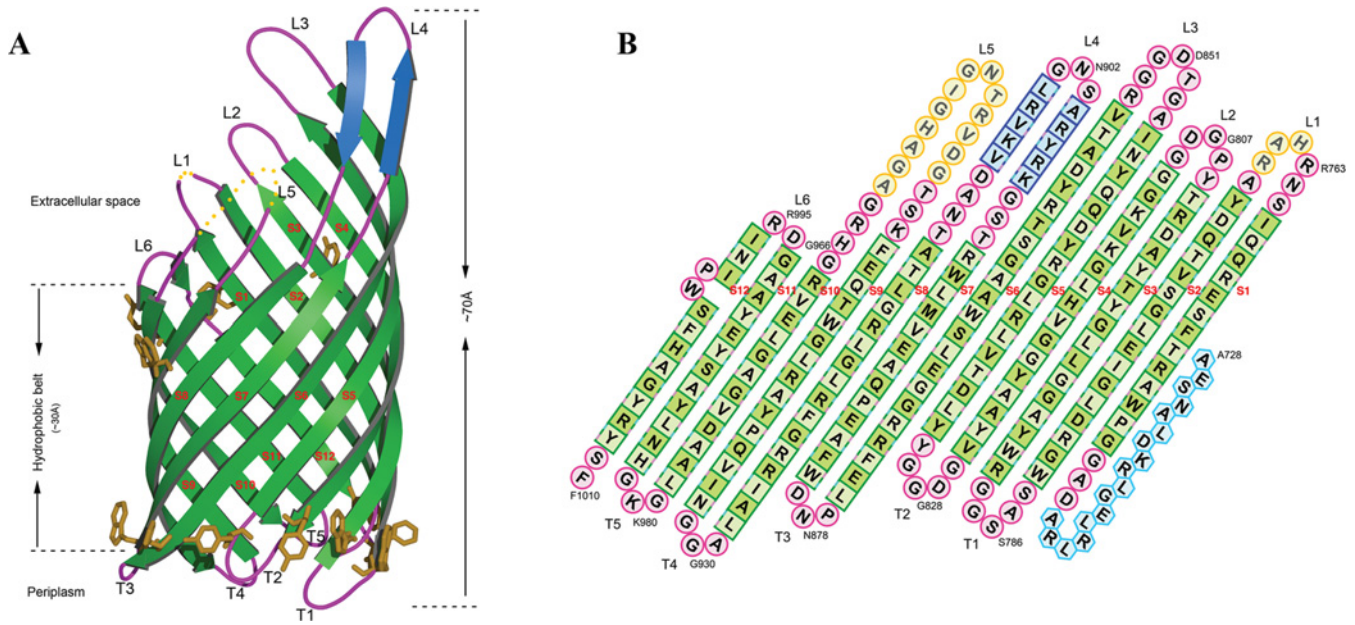

Figure 1 Overall structure and topology of BrkAβ

The β-strands (S1–S12) of the barrel are coloured green, extracellular loops (L1–L6) and periplasmic turns (T1–T5) are coloured pink, the small β-sheet of L4 is coloured blue, untraced residues of L1 and L5 are coloured yellow, and the segment inserted into the pore is coloured cyan. All of the strands, loops and turns are labelled. (**A**) Cartoon representation of BrkAβ overall structure produced using Molscript [45] and Bobscript [46]. Side chains of the aromatic girdle are shown in gold sticks. (**B**) Topology diagram of BrkAβ. The residues are numbered according to the full-length mature BrkA protein. The residues facing the barrel pore are highlighted by lime squares and those facing the lipid bilayer by light green squares.

E. coli C41(DE3) cells transformed with an empty vector or the vectors containing the above genes were grown to a D_{600} of 0.4 and induced by 0.02 mM IPTG (isopropyl β-D-thiogalactopyranoside) for 2 h at 37 °C. Then, 2 ml of culture was harvested by centrifugation at 2000 ***g*** for 10 min and resuspended in 410 μl of PBS. For 200 μl of cells, 4 μl of 10 mg/ml trypsin was added. After incubation at 37 °C for 10 min, the cells were put on ice immediately and 20 μl of FBS (fetal bovine serum) was added to stop digestion. The cells were pelleted by centrifugation at 2000 ***g*** for 5min at 4 °C, washed three times with PBS containing 10 % FBS and once in PBS alone. The washed cells were finally resuspended in 5× SDS loading buffer and boiled for 10 min. As a control, another 200 μl aliquot of cells was simultaneously processed in the same manner without added trypsin. Samples were resolved by SDS/PAGE (12 % gels) and transferred on to nitrocellulose membranes (Millipore) for 70 min at 300 mA at 4 °C. The non-secreted and secreted proteins were detected by anti-His antibody (Sigma) and horseradish peroxidase-conjugated goat anti-mouse secondary antibody (ZSGB-Bio) with a working dilution of 1:3000 and 1:2500 respectively. The membranes were incubated in luminol reagent (Santa Cruz Biotechnology) and exposed to film.

Bacterial membrane extraction and separation of OM and IM

The OM of *E. coli* expressing BrkAΔ-PC or its mutants was prepared using the methods of Filip et al. [39] and Kumar et al. [40]. Briefly, *E. coli* strain C41(DE3) cells transformed with an empty vector, or the vectors containing the above genes, were grown at 37 °C in 500 ml of 2YT [1.6 % (w/v) tryptone/1 % (w/v) yeast extract/0.5 % NaCl]/ampicillin medium. When the D_{600} of the culture reached ~0.8, IPTG was added to a final concentration of 0.02 mM and the culture was incubated further at 37 °C for 2 h. Cells were harvested by centrifugation at 6300 ***g*** for 15 min (Beckman JA10 rotor), washed with ice-cold PBS containing 10 % (v/v) glycerol and 1 mM PMSF, and resuspended in 20 ml of TE buffer (20 mM Tris/HCl, pH 8.0, and 10 mM EDTA) with protease inhibitors (Roche) added. After sonication on ice, the lysate was centrifuged at 8600 ***g*** for 10 min at 4 °C (Beckman JA25.5 rotor). The supernatant was collected and centrifuged at 20000 ***g*** for 20 min at 4 °C (Beckman JA25.5 rotor). The supernatant was collected again and ultracentrifuged at 35000 rev./min for 1 h at 4 °C (Beckman Ti 70 rotor). The pellet, which is the total membrane fraction, was homogenized with 10 ml of TE buffer. Then the sample was ultracentrifuged again at 35000 rev./min for 35 min at 4 °C (Beckman Ti 70 rotor). The pellet was homogenized with 4 ml of TE buffer, and the total protein concentration was determined using the BCA method. The protein concentration was adjusted to 5 mg/ml and solubilized by sarkosyl with a final concentration of 1 % (w/v) at 4 °C for 1 h. In this step, the IM could be resolved into the solubilized supernatant. After ultracentrifugation at 35000 rev./min for 1 h at 4 °C (Beckman Ti 70 rotor), the sarkosyl-insoluble OM fraction was homogenized in 2 ml of TE buffer. The total protein concentrations of both the IM and OM fractions were determined using the BCA method and adjusted to 1 mg/ml using TE buffer. Samples were resolved by SDS/PAGE (12 % gels) and subjected to Western blot analysis.

RESULTS AND DISCUSSION

Overall structure of BrkAβ

Purified refolded BrkAβ was crystallized in space group $C222_1$, and its crystal structure was determined by MR and refined at 3.0 Å resolution with R_{work} 26.6 % and R_{free} 32.4 % (Table 1). The overall structure of BrkAβ (residues Ala^{728}–Phe^{1010}) is a 12-stranded antiparallel β-barrel with a height of ~70 Å and an ellipsoidal cross section of ~19 Å×27 Å (Figure 1A). The interior of the

Table 2 Description of mutant BrkA constructs

Construct name	Mutation sites	Description
BrkAΔ-1	Deletion of residues Lys^{896}–Val^{908} of L4	Deletion of L4
BrkAΔ-2	Deletion of residues Asp^{951}–Gly^{963} of L5	Deletion of L5
BrkAΔ-3	R899D, R905D and R907D	Mutation of basic residues on L4 to acidic residues
BrkAΔ-4	Y898D, A900D, L904D, V906D and V908D	Mutation of all hydrophobic residues on L4 to acidic residues
BrkAΔ-5	Y898K, A900K, L904K, V906K and V908K	Mutation of all hydrophobic residues on L4 to basic residues
BrkAΔ-6	Y845D and I847D	Mutation of two hydrophobic residues on S5 to acidic residues
BrkAΔ-7	V855D, A857D and Y859D	Mutation of three hydrophobic residues on S6 to acidic residues
BrkAΔ-8	Y768D	Mutation of only one hydrophobic residue on S2 in the hydrophobic cavity to an acidic residue
BrkAΔ-9	Y805D	Mutation of only one hydrophobic residue on S3 in the hydrophobic cavity to an acidic residue
BrkAΔ-10	Y845D, I847D, V855D, A857D and Y859D	BrkAΔ-6+BrkAΔ-7, mutation of all relevant hydrophobic residues on S5 and S6 to acidic residues
BrkAΔ-11	Y805D, Y845D, I847D, V855D, A857D and Y859D	BrkAΔ-6+BrkAΔ-7+BrkAΔ-9, mutation of most hydrophobic residues around S5 and S6 to acidic residues
BrkAΔ-12	Y768D, Y805D, Y845D, I847D, V855D, A857D and Y859D	BrkAΔ-6+BrkAΔ-7+BrkAΔ-8+BrkAΔ-9, mutation of most hydrophobic residues around S5 and S6 to acidic residues

β-barrel is packed with 37 hydrophilic and 34 hydrophobic residues. The exterior of the β-barrel is composed of a hydrophobic belt that is lined by two girdles of aromatic residues at the top and bottom (Figure 1A). The width of the hydrophobic belt (∼30 Å) is complementary to the non-polar portion of the OM (Figure 1A). The β-barrel has a shear number of 14, and the β-strands are tilted at an angle of ∼45° to the barrel axis (Figure 1B). The β-strands (S1–S12) range in length from 11 to 22 residues and are connected by short periplasmic turns (T1–T5) and extracellular loops (L1–L6) of various lengths (Figure 1). The longest loop (L4 or L5) contains 20 residues, whereas the shortest loop (L6) contains only two residues. L1 and L5 cannot be completely built because of the poor electron density, indicating their structural flexibility. In L4, two antiparallel β-strands form a small β-sheet and protrude into the extracellular space. A short loop before the first strand of the β-barrel is inserted into the central pore from the periplasmic side. Although an elongated stretch of electron density is present in the pore, it is too smeared to trace any residues before Asp^{745} (Figure 1B and see Supplementary Figure S2). Since black lipid bilayer experiments indicated the processing of the passenger domain of BrkA occurs at the site between Asn^{731} and Ala^{732} [10,11,16], i.e. before Asp^{745}, it is further believed that the passenger domain is cleaved inside the central pore of the BrkA β-barrel.

A hairpin-like structure formed by L4 inserts into an adjacent pore for crystal packing

In the crystal structure of BrkAβ, there are three molecules per asymmetric unit. They adopt almost identical conformations and superimpose well with the RMSD (root mean square deviation) less than 0.8 Å (see Supplementary Figure S3 at http://www.BiochemJ.org/bj/435/bj4350577add.htm). Within one asymmetric unit, two molecules (M1 and M2) form a pseudo-dimer (D1), whereas the third (M3) forms an identical pseudo-dimer (D2) with a molecule from an adjacent asymmetric unit (M4) (Figure 2). Within such a pseudo-dimer, the small β-sheet of L4 from one monomer inserts into the hydrophobic cavity of the other monomer and forms a hairpin-like structure located exactly over the extracellular entrance of the β-domain pore. The side chains of Tyr^{898}, Ala^{900}, Leu^{904}, Val^{906} and Val^{908} on the small β-sheet are involved in hydrophobic interactions with the hydrophobic patches on S5 (Tyr^{845} and Ile^{847}) and S6 (Val^{855}, Ala^{857} and Tyr^{859}) of the second molecule. Although there are tight hydrophobic interactions within these pseudo-dimers, SEC-MALS demonstrated that BrkAβ exists as a monomer under different detergent conditions, even for the detergent C_8E_4 that was used for crystallization (see Supplementary Figure S4 at http://www.BiochemJ.org/bj/435/bj4350577add.htm). That suggests the dimer formation observed results from the crystal packing. The monomeric state of BrkAβ is in accordance with other reported AT β-domains [24,41,42]. However, the fact that L4 could be inserted into the adjacent monomer at least indicates that the hairpin structural motif could be accommodated properly within the central pore, which has been suspected for a long time.

Structural comparison with other AT β-domains

Before the present study, there were only three available structures for AT β-domains: Nalpβ from *N. meningitidis* (PDB code 1UYN) [24], EspPβ from *E. coli* strain O157:H7 (PDB code 2QOM) [25] and EstAβ from *Ps. aeruginosa* (PDB code 3KVN) [26]. Although BrkAβ shares low sequence homology with them (<25 % identity), its overall structure is similar to Nalpβ, EspPβ and EstAβ with Cα RMSDs of 2.3, 1.7 and 2.6 Å respectively (see Supplementary Figure S5 at http://www.BiochemJ.org/bj/435/bj4350577add.htm). On L4 of BrkAβ, the small β-sheet (residues 896–908) contains alternating basic and hydrophobic residues. Those hydrophobic residues (Tyr^{898}, Ala^{900}, Leu^{904}, Val^{906} and Val^{908}) are oriented into the interior of the pore and form a hydrophobic cavity with the opposite extracellular hydrophobic residues (Tyr^{768}, Tyr^{805}, Tyr^{845}, Ile^{847}, Val^{855}, Ala^{857} and Tyr^{859}) on S2, S3, S5 and S6 (Figures 3A and 3B). Interestingly, similar hydrophobic regions are also found in other AT β-domains of Nalpβ, EspPβ and EstAβ (Figures 3C, 3D and 3E), but never reported before, presumably because of a lack of structures to be compared. Although the residues forming the hydrophobic regions are not conserved among these AT β-domains, the common hydrophobic cavity feature in their extracellular entrance of the pore suggests a relationship with the mechanism of AT secretion.

Hydrophobic patches of L4, S5 and S6 are required for passenger domain translocation of BrkA

It has been reported that the cleaved passenger domain of BrkA remains tightly associated with the bacterial surface after secretion and is not detected in *B. pertussis* culture supernatants. As a result, both the unprocessed precursor and the cleaved passenger domain can be detected by anti-BrkA serum in the whole-cell lysates [16]. Furthermore, the surface-associated passenger domain could be accessed and digested by trypsin added to the culture. This kind

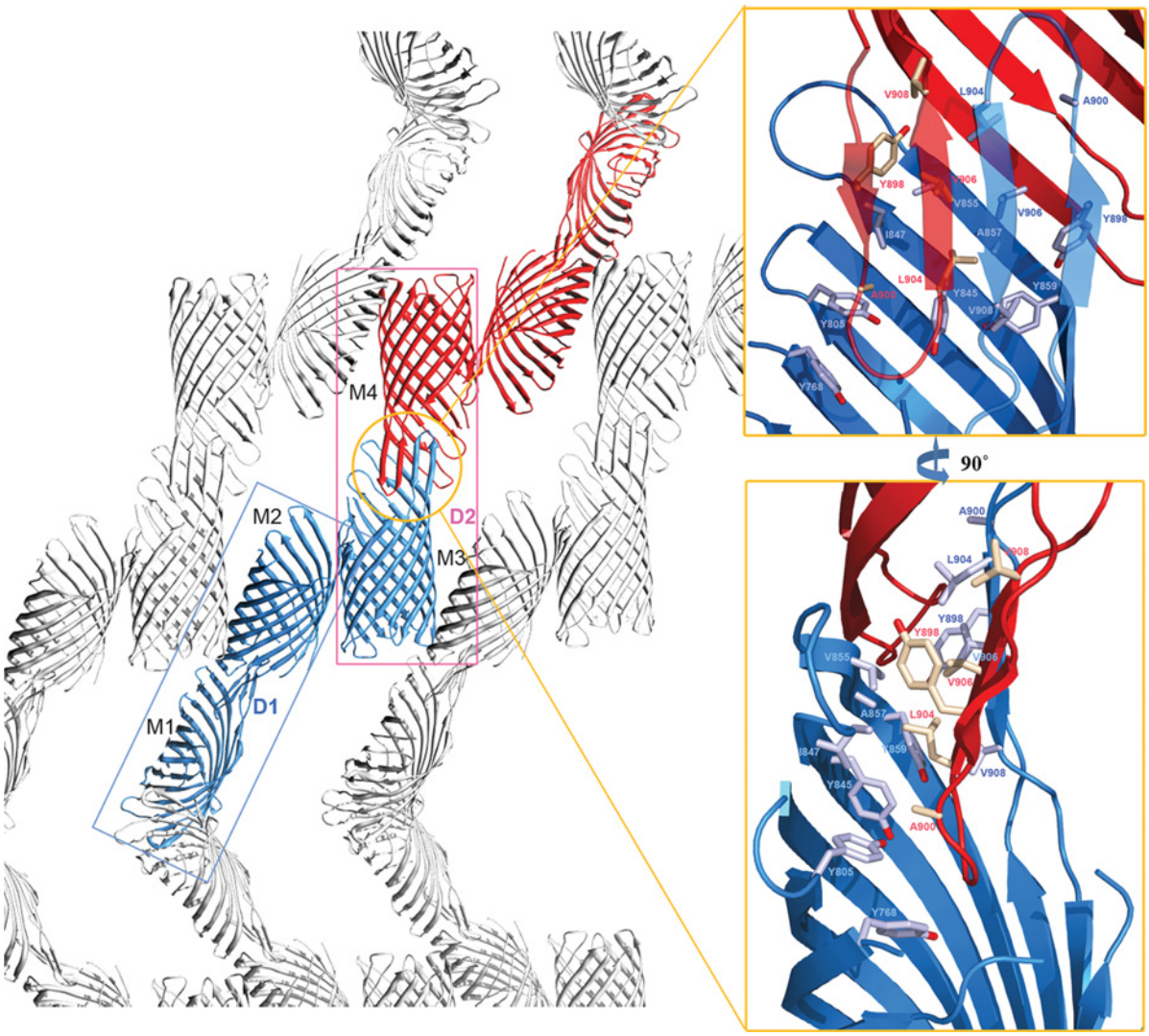

Figure 2 Crystal packing results in a hairpin-like structure above the central pore

Crystal packing of BrkAβ in space group $C222_1$. Molecules in one asymmetric unit are labelled and shown in blue (M1, M2 and M3) and their neighbours are in red (M4, M5 and M6). The two types of pseudo-dimers (D1 and D2) are indicated by blue and pink squares respectively. The detailed hydrophobic interactions within D2 are shown in the top-right and bottom-right insets. The bottom-right inset is rotated vertically anticlockwise by 90° with respect to the top-right one. Side chains of the hydrophobic residues involved in the D2 interaction interface are shown as sticks, coloured light magenta for M3 and light yellow for M4 and labelled accordingly. The left-hand panel for crystal packing was made by using UCSF Chimera [47] and the insets were produced using PyMOL (http://www.pymol.org).

of trypsin-accessibility assay has been widely used to study the secretion/translocation state of prokaryotic proteins [9,43,44].

The role of the hydrophobic cavity in the passenger domain translocation of BrkA could be studied by expressing BrkA and a series of mutants with modified hydrophobic patches (Table 2) in *E. coli* (a similar Gram-negative bacterium to *B. pertussis* with the same virulence factor secretion mechanism) and using the trypsin-accessibility approach to investigate whether the mutants have decreased or destroyed passenger domain translocation activity. However, overexpression of the full-length BrkA protein in *E. coli* is lethal [16], although it has been shown that the upstream 31–39-residue region preceding BrkAβ is essential and sufficient for passenger domain translocation [9]. Accordingly, we cloned a new construct BrkAΔ-PC for positive control (similar to the BrkA deletion construct E in [9]), in which Gln^{60}–Asp^{544} in the BrkA passenger domain were deleted and a His_6 tag was inserted between Gly^{59} and Ala^{545} to produce a 57 kDa precursor (preBrkA) with an unprocessed signal peptide, a 52 kDa mature full-length protein (BrkA) and a 22 kDa passenger domain (Figure 4A). As shown in Figure 4(B), for BrkAΔ-PC without trypsin treatment, both the 52 kDa full-length protein and the 22 kDa cleaved passenger domain can be detected by an anti-His antibody. Treating the whole cells with trypsin resulted in the complete digestion of the 22 kDa moiety, indicating that BrkAΔ-PC could successfully secrete its passenger domain to the bacterial surface in a manner similar to the wild-type BrkA. Because it will normally take several minutes to complete the passenger domain secretion process [29], the 52 kDa full-length protein represents the intermediates inaccessible to trypsin, which is located in the periplasm or only targeted to the OM without passenger domain translocation. After trypsin treatment, the amount of the 52 kDa band is decreased, which is believed to be due to further secretion occurring during trypsin treatment. The membrane localization of expressed BrkAΔ-PC was visualized

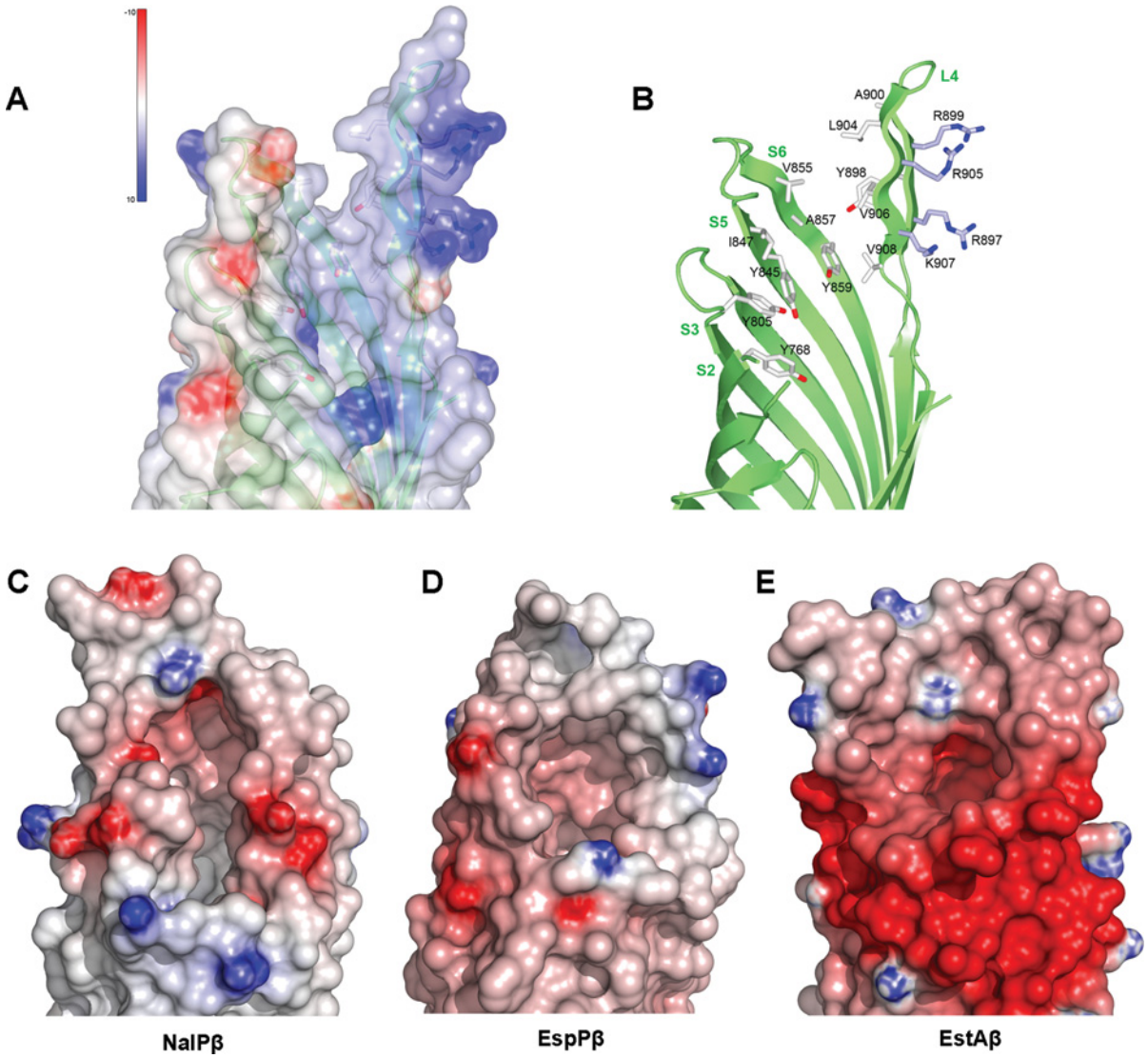

Figure 3 Extracellular hydrophobic cavities of AT β-domains

(**A**) The extracellular hydrophobic cavity in BrkAβ is shown with an electrostatic potential surface. (**B**) The labelled hydrophobic residues forming the cavity are shown as white sticks and the basic residues of L4 are shown as slate sticks. S2, S3, S5 and S6, and L4 are labelled accordingly. For comparison, electrostatic potential surfaces of NalPβ (**C**), EspPβ (**D**) and EstAβ (**E**) respectively are shown in the same orientation as BrkAβ. The electrostatic potential was calculated by DelPhi [48] and all structures were produced using PyMOL (http://www.pymol.org).

by immunoelectron microscopy (see Supplementary Figure S6 at http://www.BiochemJ.org/bj/435/bj4350577add.htm) and confirmed by statistical nanogold counting (see Supplementary Table S1 at http://www.BiochemJ.org/bj/435/bj4350577add.htm). All of the above demonstrates that BrkAΔ-PC is a rational positive control to study the passenger domain translocation mechanism using the trypsin-accessibility assay.

To determine the effect of the small β-sheet of L4 on the translocation of the passenger domain, we made a truncation mutant BrkAΔ-1 in which Lys^{896}–Val^{908} were deleted from BrkAΔ-PC (Figure 3B and Table 2). Although the 22 kDa passenger domain was detected for BrkAΔ-1, the ratio of its amount to that of the 52 kDa moiety is much lower than that of BrkAΔ-PC (Figure 4B), indicating that the translocation efficiency of BrkAΔ-1 passenger domain was largely reduced. To investigate whether the decrease in translocation efficiency would result from the removal of an extracellular loop, another truncation mutant BrkAΔ-2 was made in which Asp^{951}–Gly^{963} of L5 were deleted from BrkAΔ-PC (Figure 1B and Table 2). No effect on passenger domain translocation of this mutant could be found (Figure 4B), which is consistent with that of EspPβ1 (βL5) [25]. These data indicate the small β-sheet of L4 is required for efficient translocation of the passenger domain.

To examine whether the hydrophobic or basic residues on the small β-sheet in L4 (Figure 3B) contribute to the translocation effect, we made three mutants from BrkAΔ-PC. One mutant, BrkAΔ-3, which contains three point mutations, R899D, R905D and R907D (Figure 3B and Table 2), can successfully translocate its passenger domain to the bacterial surface with no distinct difference from BrkAΔ-PC (Figure 4B). However, no cleaved passenger domain can be detected in the other two mutants, BrkAΔ-4 and BrkAΔ-5 (Figure 4B), in which the hydrophobic residues (Tyr^{898}, Ala^{900}, Leu^{904}, Val^{906} and Val^{908}) in the small β-sheet were each mutated to aspartate and lysine respectively (Figure 3B and Table 2). These data suggest that it is the hydrophobic surface and not the positive electrostatic surface of

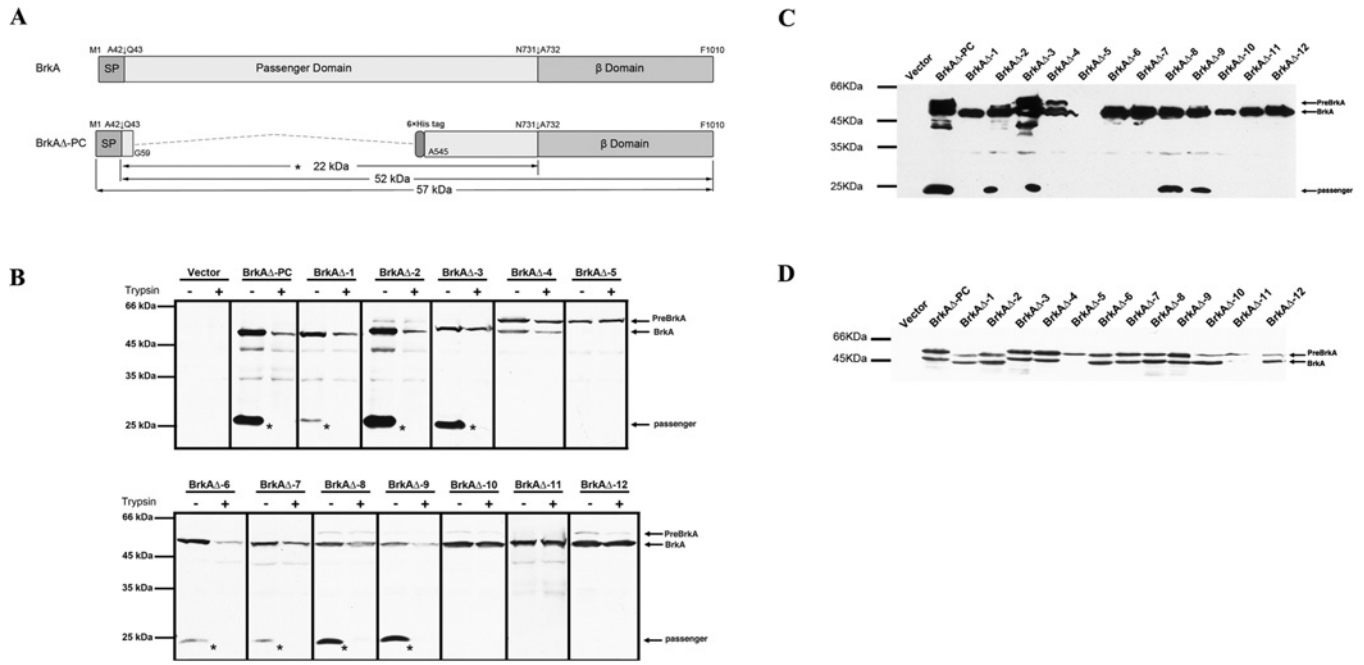

Figure 4 Construction of BrkAΔ-PC, and trypsin-accessibility and membrane localization assays

(**A**) BrkA domain organization and the construct design of BrkAΔ-PC. SP, signal peptide. The inserted His_6 tag is depicted as a grey square. Both the signal peptide-processing site and the passenger domain cleavage site are indicated by black arrows. All other labels are self-explanatory. (**B**) Results of trypsin-accessibility assay for BrkAΔ-PC and its mutants. Cells were processed in the presence (+) or absence (−) of trypsin as described in the Experimental section. (**C**) Detection of BrkAΔ-PC and its mutants in the OM. (**D**) Detection of BrkAΔ-PC and its mutants in the IM. Descriptions of all of the mutants in (**B**), (**C**) and (**D**) are found in Table 2. The band positions for the precursor (PreBrkA), the mature full-length protein (BrkA) and the cleaved passenger domain (passenger) are indicated by black arrows and labelled accordingly in (**B**), (**C**) and (**D**). Molecular masses are indicated in kDa.

the small β-sheet that is essential for the translocation of the passenger domain.

To assess further the role of the extracellular hydrophobic cavity (Figure 3A) of BrkAβ for passenger domain translocation, mutations of other hydrophobic residues on the cavity were made from BrkAΔ-PC. Located in the central region of the cavity, the hydrophobic residues on S5 (Tyr^{845} and Ile^{847}) and S6 (Val^{855}, Ala^{857} and Tyr^{859}) were each replaced by aspartate in BrkAΔ-6 and BrkAΔ-7 respectively (Figure 3B and Table 2). The severe translocation inability of those mutants (Figure 4B) revealed that the hydrophobicity of the cavity is required for translocation. To test this hypothesis further, more hydrophobic residues of the cavity were each mutated to aspartate simultaneously so that the cavity hydrophobicity could be reduced further. As expected, for those mutants BrkAΔ-10, BrkAΔ-11 and BrkAΔ-12 (Figure 3B and Table 2), no cleaved passenger domain can be detected at all (Figure 4B). In contrast, two single mutations, BrkAΔ-8 and BrkAΔ-9 (Figure 3B and Table 2), where only one selected hydrophobic residue on S2 or S3 in the cavity is mutated to an acidic residue, did not affect passenger domain translocation significantly (Figure 4B), possibly because the two residues are located in the peripheral region of the hydrophobic cavity and the single mutation does not affect its overall hydrophobicity. These data show that the hydrophobic surface of the cavity formed by at least Tyr^{845}, Ile^{847}, Val^{855}, Ala^{857} and Tyr^{859} on S5 and S6 is essential for the translocation of the passenger domain.

To assess the possibility that the failure to detect the cleaved passenger domain in the whole-cell lysates of the above mutants is due to an attenuated interaction between the β-domain and the cleaved passenger domain that is eventually released to cell culture, the medium supernatants of cultured bacteria expressing BrkAΔ-PC and all its mutants were analysed by dot blotting. No cleaved passenger domain could be detected from the bacterial culture (results not shown).

Another concern might be whether those mutations affect the membrane localization of the expressed protein. Using the same protocol for BrkAΔ-PC (see Supplementary Figure S6), we took hundreds of electron micrographs to visualize the immunolabelled sections of bacteria that expressed the mutants. Compared with the bacteria containing only the empty vector, there are significant nanogolds localized on the bacterial membrane for all of the mutants, although there are also enough nanogolds counted in the plasma (results not shown). This suggests that enough protein for all BrkAΔ-PC mutants folds correctly and is efficiently localized on to the membrane. It should be noted that it is not unusual to find the BrkA protein in the plasma of *E. coli* (see Supplementary Figure S6) because overexpression of BrkA will yield abundant inclusion bodies in the plasma and the BrkAβ protein in the present study was actually purified and refolded from inclusion body.

Although the immunolabelling electron microscopy demonstrated the membrane localization of BrkAΔ-PC and its mutants, it could be argued that defects in passenger domain secretion might be caused by a failure of the mutants to be correctly targeted to the OM, rather than a dysfunction of the β-domain translocation ability. To clarify, the bacterial membranes were extracted and separated into the IM and OM fractions according to the previously reported and widely used protocol [39,40]. As shown in Figure 4(C), with the exception of BrkAΔ-5, the 52 kDa mature full-length protein of all other mutants could be clearly detected in the OM fraction, and, for most of them, the precursor proteins (57 kDa moiety) could not be detected at all. The cleaved passenger domain could also be clearly identified for those BrkA proteins (BrkAΔ-PC, BrkAΔ-2, BrkAΔ-3, BrkAΔ-8 and BrkAΔ-9) that have significant passenger domain

translocation activity. Furthermore, all of the BrkA proteins could be found from the IM fraction (Figure 4D) and most of them exhibited two bands, one of which (57 kDa moiety) represents the precursor (preBrkA) with the signal peptide unprocessed and the other (52 kDa moiety) representing the mature full-length protein (BrkA) that has been translocated across the IM via the Sec-pathway and has not been targeted to the OM. Interestingly, although BrkAΔ-5 could not be found in the OM fraction, it can be clearly detected as the precursor form in the IM fraction (Figure 4D), which is consistent with the observation that only the precursor band could be found in the trypsin-accessibility experiments (Figure 4B).

Taking all of the above data together, we can conclude that, except for BrkAΔ-5, all the BrkA proteins in the present study can be correctly localized into the OM and the undetected cleaved passenger domain in the trypsin accessibility assay is due to the failure of the BrkAβ translocation ability, which is caused by the destruction of the hydrophobic cavity formed by L4, S5 and S6. For BrkAΔ-5, we speculate that changing the hydrophobic residues of L4 to basic ones (BrkAΔ-5, Table 2), not to acidic ones (BrkAΔ-4, Table 2), will alter the tertiary structure of BrkA significantly, preventing its correct translocation across the IM via a Sec-dependent pathway.

Implications for the secretion mechanism of ATs

We have described the crystal structure of BrkAβ and assessed the essential role of the hydrophobic cavity, formed by the hydrophobic patches of L4 (Tyr^{898}, Ala^{900}, Leu^{904}, Val^{906} and Val^{908}), S5 (Tyr^{845} and Ile^{847}) and S6 (Val^{855}, Ala^{857} and Tyr^{859}), for the passenger domain translocation. Our experiments have shown that disruption of any one of these hydrophobic patches will result in a remarkable decrease in translocation efficiency. After a comparison with other available structures of the classical AT β-domains, we found that the hydrophobic cavity formed by S5, S6 and L4 exhibits a ubiquitous structural characteristic of the extracellular part of the β-domain, despite the low sequence homology (Figures 3A, 3C, 3D and 3E). This structural conservation might play a role in the secretion mechanism of AT passenger domain.

As addressed above, there are four proposed models for the AT passenger domain translocation: (i) the threading model, (ii) the hairpin model [18], (iii) the multimer model [31], and (iv) the Omp85-mediated model [28]. The lack of specific N-terminal motifs to target the pore makes the threading model unlikely [28,29]. The multimer model can also be challenged as a general mechanism, since most AT β-domains, as well as the BrkAβ in the present study, were reported in the monomeric state [24,41,42], and it is difficult for β-barrels with hydrophobic exteriors to form a hydrophilic channel [28]. Recent studies have provided evidence to support the Omp85-mediated model [29] and the hairpin model [30]. Ieva et al. [29] reported that the C-terminal polypeptide segment of the passenger domain is embedded into the β-domain pore in the periplasmic space before targeting the OM. Although this suggests that the passenger domains might be translocated across the OM by a concerted mechanism via exogenous factors such as the Omp85 complex, their data do not exclude the hairpin model. Recently, Junker et al. [30] introduced pairs of cysteine residues into the sequence of the pertactin passenger domain and showed that the C-terminus of the domain firstly emerges across the OM before forming a stable folded form. In the context of the hairpin model, this suggests that the C-terminus of the passenger domain forms a stable core first and thereby provides a template of β-strands to promote fast folding and translocation of the proximal N-terminal portions through the pore [30].

The results of the present study do not exclude either the Omp85-mediated model or the hairpin model, but provide more implications for these two mechanisms. Figure 4 shows that, although some mutants (BrkAΔ-4, BrkAΔ-10, BrkAΔ-11 and BrkAΔ-12) totally lose their passenger domain translocation activity, they could also be efficiently targeted into the OM, suggesting that altering the extracellular hydrophobic cavity of the β-domain does not affect its OM localization. If the Omp85-mediated model is correct, although alteration of the hydrophobic cavity might inhibit the C-terminal segment of the passenger domain from being correctly inserted into the β-domain pore, the inability to form a stable intermediate does not influence its interaction with an Omp85 complex and its integration into the OM. However, the question of why the passenger domain could not be translocated across the OM when the protein has been correctly loaded on to the OM remains. In contrast, our observations are more compatible with the hairpin model. First, although the hairpin-like structural motif observed in the present study results from crystal packing, it at least suggests that this kind of structural motif could be properly accommodated within the pore, which has been argued for many years. Secondly, following the work by Junker et al. [30] showing that the C-terminus is the first portion of the pertactin passenger domain to cross the OM before forming a stable structure, we speculate that the extracellular hydrophobic cavity might provide a favourable environment to anchor the hairpin-like hydrophobic structural motif and thereby promote fast and efficient folding of subsequently secreted N-terminal portions of the passenger domain. There remains the question of why the mutant BrkAΔ-4, in which the hydrophobic residues of L4 were replaced by acidic residues, can inhibit translocation more efficiently than BrkAΔ-1, an L4 deletion mutant. The reason might be that more electrostatic charges in the former mutant influence the overall hydrophobicity of the cavity more severely than a deletion of the loop. Presumably, the passenger domain secretion mechanism of AT might derive from both the Omp85 model and the hairpin model, as indicated previously by Bernstein (in Figure 3b of [28]). In the periplasm, the passenger domain C-terminal segment is initially incorporated into the β-domain pore and forms a hairpin-like structure that is protected by periplasmic chaperone proteins. Following this, the β-domain pore is integrated on to the OM with the aid of Omp85. After integrating into the OM, the hairpin-like structural motif will provide a template of β-strands to initiate passenger domain translocation whose completion could perhaps be driven by the β-helix folding of the passenger domain on the surface.

Many ATs have been shown, or proposed, to be virulence factors essential for the pathogenesis of disease-causing bacteria. Understanding how virulence factors are secreted and the elucidation of the atomic structures of ATs are of great importance. Inhibition of the virulence factor translocation may provide a possible therapeutic approach to block colonization by limiting the expression of functional virulence factors on the pathogens. The identified hydrophobic cavity formed by L4 (Tyr^{898}, Ala^{900}, Leu^{904}, Val^{906} and Val^{908}), S5 (Tyr^{845} and Ile^{847}) and S6 (Val^{855}, Ala^{857} and Tyr^{859}) of BrkAβ provides such a potential target for anti-pertussis drug design and gives a new direction in the study of AT translocation mechanisms.

AUTHOR CONTRIBUTION

Neil Isaacs and Xujia Zhang initiated the project. Isobel Black, Yanshi Zhu and Yanwu Huo cloned and purified the protein and obtained the first crystals. Yujia Zhai and Yanwu Huo performed the crystallization optimization and screening. Yanshi Zhu and Aleksander Roszak collected and processed diffraction data at the ESRF. Yujia Zhai and Qiangjun

Zhou collected diffraction data at Shanghai. Yujia Zhai and Kai Zhang processed the data and solved the crystal structure. Yujia Zhai performed all of the mutagenesis and biochemical studies with the help of Xiaoyun Pang. Jiuwei Lu finished the immunolabelling experiments. Yujia Zhai and Fei Sun analysed the data and wrote the paper. Neil Isaacs, Yanshi Zhu and Aleksander Roszak contributed to the editing and revising of the paper before submission. Fei Sun and Neil Isaacs supervised the whole project.

ACKNOWLEDGEMENTS

We thank Professor Rachel Fernandez from the University of British Columbia for supplying us with the plasmid pD06935 containing the full-length *BrkA* gene. We are grateful to Jun Ma and Yingzhi Xu (F.S.'s group) for their help on cloning mutants and Western blot experiments. We also thank Xudong Zhao, Ruimin Zheng and Su Liu (Core Facilities for Protein Sciences, Chinese Academy of Sciences) for their group's help on maintaining the instruments in our laboratory. We acknowledge the ESRF, Grenoble, France, for the provision of synchrotron radiation facilities and thank Dr Gianluca Cioci for assistance in using beamline ID29.

FUNDING

This work was supported by the National Science Foundation of China [grant numbers 30970569 and 30721003], the '973' project of the Chinese Ministry of Science and Technology [grant numbers 2006CB911001, 2006CB806506 and 2009CB918803] and a Partnering China Award from the Biotechnology and Biological Sciences Research Council.

REFERENCES

1 Anon (2006) Challenges in global immunization and the Global Immunization Vision and Strategy 2006–2015. Wkly. Epidemiol. Rec. **81**, 190–195
2 Crowcroft, N. S., Stein, C., Duclos, P. and Birmingham, M. (2003) How best to estimate the global burden of pertussis? Lancet Infect. Dis. **3**, 413–418
3 Tanaka, M., Vitek, C. R., Pascual, F. B., Bisgard, K. M., Tate, J. E. and Murphy, T. V. (2003) Trends in pertussis among infants in the United States, 1980–1999. JAMA, J. Am. Med. Assoc. **290**, 2968–2975
4 Forsyth, K. D., Wirsing von Konig, C. H., Tan, T., Caro, J. and Plotkin, S. (2007) Prevention of pertussis: recommendations derived from the second Global Pertussis Initiative roundtable meeting. Vaccine **25**, 2634–2642
5 Fernandez, R. C. and Weiss, A. A. (1994) Cloning and sequencing of a *Bordetella pertussis* serum resistance locus. Infect. Immun. **62**, 4727–4738
6 Weiss, A. A. and Goodwin, M. S. (1989) Lethal infection by *Bordetella pertussis* mutants in the infant mouse model. Infect. Immun. **57**, 3757–3764
7 Elder, K. D. and Harvill, E. T. (2004) Strain-dependent role of BrkA during *Bordetella pertussis* infection of the murine respiratory tract. Infect. Immun. **72**, 5919–5924
8 Marr, N., Oliver, D. C., Laurent, V., Poolman, J., Denoel, P. and Fernandez, R. C. (2008) Protective activity of the *Bordetella pertussis* BrkA autotransporter in the murine lung colonization model. Vaccine **26**, 4306–4311
9 Oliver, D. C., Huang, G. and Fernandez, R. C. (2003) Identification of secretion determinants of the *Bordetella pertussis* BrkA autotransporter. J. Bacteriol. **185**, 489–495
10 Shannon, J. L. and Fernandez, R. C. (1999) The C-terminal domain of the *Bordetella pertussis* autotransporter BrkA forms a pore in lipid bilayer membranes. J. Bacteriol. **181**, 5838–5842
11 Passerini de Rossi, B. N., Friedman, L. E., Gonzalez Flecha, F. L., Castello, P. R., Franco, M. A. and Rossi, J. P. (1999) Identification of *Bordetella pertussis* virulence-associated outer membrane proteins. FEMS Microbiol. Lett. **172**, 9–13
12 Brandon, L. D., Goehring, N., Janakiraman, A., Yan, A. W., Wu, T., Beckwith, J. and Goldberg, M. B. (2003) IcsA, a polarly localized autotransporter with an atypical signal peptide, uses the Sec apparatus for secretion, although the Sec apparatus is circumferentially distributed. Mol. Microbiol. **50**, 45–60
13 Sijbrandi, R., Urbanus, M. L., ten Hagen-Jongman, C. M., Bernstein, H. D., Oudega, B., Otto, B. R. and Luirink, J. (2003) Signal recognition particle (SRP)-mediated targeting and Sec-dependent translocation of an extracellular *Escherichia coli* protein. J. Biol. Chem. **278**, 4654–4659
14 Peterson, J. H., Szabady, R. L. and Bernstein, H. D. (2006) An unusual signal peptide extension inhibits the binding of bacterial presecretory proteins to the signal recognition particle, trigger factor, and the SecYEG complex. J. Biol. Chem. **281**, 9038–9048
15 Dautin, N., Barnard, T. J., Anderson, D. E. and Bernstein, H. D. (2007) Cleavage of a bacterial autotransporter by an evolutionarily convergent autocatalytic mechanism. EMBO J. **26**, 1942–1952
16 Oliver, D. C. and Fernandez, R. C. (2001) Antibodies to BrkA augment killing of *Bordetella pertussis*. Vaccine **20**, 235–241
17 Pohlner, J., Halter, R., Beyreuther, K. and Meyer, T. F. (1987) Gene structure and extracellular secretion of *Neisseria gonorrhoeae* IgA protease. Nature **325**, 458–462
18 Henderson, I. R., Navarro-Garcia, F. and Nataro, J. P. (1998) The great escape: structure and function of the autotransporter proteins. Trends Microbiol. **6**, 370–378
19 Emsley, P., Charles, I. G., Fairweather, N. F. and Isaacs, N. W. (1996) Structure of *Bordetella pertussis* virulence factor P. 69 pertactin. Nature. **381**, 90–92
20 Otto, B. R., Sijbrandi, R., Luirink, J., Oudega, B., Heddle, J. G., Mizutani, K., Park, S. Y. and Tame, J. R. (2005) Crystal structure of hemoglobin protease, a heme binding autotransporter protein from pathogenic *Escherichia coli*. J. Biol. Chem. **280**, 17339–17345
21 Junker, M., Schuster, C. C., McDonnell, A. V., Sorg, K. A., Finn, M. C., Berger, B. and Clark, P. L. (2006) Pertactin β-helix folding mechanism suggests common themes for the secretion and folding of autotransporter proteins. Proc. Natl. Acad. Sci. U.S.A. **103**, 4918–4923
22 Kajava, A. V. and Steven, A. C. (2006) The turn of the screw: variations of the abundant β-solenoid motif in passenger domains of Type V secretory proteins. J. Struct. Biol. **155**, 306–315
23 Gangwer, K. A., Mushrush, D. J., Stauff, D. L., Spiller, B., McClain, M. S., Cover, T. L. and Lacy, D. B. (2007) Crystal structure of the *Helicobacter pylori* vacuolating toxin p55 domain. Proc. Natl. Acad. Sci. U.S.A. **104**, 16293–16298
24 Oomen, C. J., van Ulsen, P., van Gelder, P., Feijen, M., Tommassen, J. and Gros, P. (2004) Structure of the translocator domain of a bacterial autotransporter. EMBO J. **23**, 1257–1266
25 Barnard, T. J., Dautin, N., Lukacik, P., Bernstein, H. D. and Buchanan, S. K. (2007) Autotransporter structure reveals intra-barrel cleavage followed by conformational changes. Nat. Struct. Mol. Biol. **14**, 1214–1220
26 Van Den Berg, B. (2010) Crystal structure of a full-length autotransporter. J. Mol. Biol. **396**, 627–633
27 Nummelin, H., Merckel, M. C., Leo, J. C., Lankinen, H., Skurnik, M. and Goldman, A. (2004) The *Yersinia* adhesin YadA collagen-binding domain structure is a novel left-handed parallel β-roll. EMBO J. **23**, 701–711
28 Bernstein, H. D. (2007) Are bacterial 'autotransporters' really transporters? Trends Microbiol. **15**, 441–447
29 Ieva, R., Skillman, K. M. and Bernstein, H. D. (2008) Incorporation of a polypeptide segment into the β-domain pore during the assembly of a bacterial autotransporter. Mol. Microbiol. **67**, 188–201
30 Junker, M., Besingi, R. N. and Clark, P. L. (2009) Vectorial transport and folding of an autotransporter virulence protein during outer membrane secretionMolMicrobiol. **71**, 1323–1332
31 Veiga, E., Sugawara, E., Nikaido, H., de Lorenzo, V. and Fernandez, L. A. (2002) Export of autotransported proteins proceeds through an oligomeric ring shaped by C-terminal domains. EMBO J. **21**, 2122–2131
32 Li, Z., Zhai, Y., Fang, J., Zhou, Q., Geng, Y. and Sun, F. (2010) Purification, crystallization and preliminary crystallographic analysis of very-long-chain acyl-CoA dehydrogenase from *Caenorhabditis elegans*. Acta Crystallogr. Sect. F Struct. Biol. Cryst. Commun. **66**, 426–430
33 Li, Z., Kai, Z., Yujia, Z., Qiangjun, Z., Yunqi, G. and Fei, S. (2010) Cloning, expression, purification and preliminary crystallographic analysis of *Caenorhabditis elegans* enoyl-CoA hydratase. Acta Biophys. Sin. **26**, 37–48
34 Paithankar, K. S. and Garman, E. F. (2010) Know your dose: RADDOSE. Acta Crystallogr. Sect. D Biol. Crystallogr. **66**, 381–388
35 Otwinowski, Z. and Minor, W. (1997) Processing of X-ray diffraction data collected in oscillation mode. Methods Enzymol. **276**, 307–326
36 Vagin, A. and Teplyakov, A. (2010) Molecular replacement with MOLREP. Acta Crystallogr. Sect. D Biol. Crystallogr. **66**, 22–25
37 Brunger, A. T. (2007) Version 1.2 of the Crystallography and NMR system. Nat. Protoc. **2**, 2728–2733
38 Winn, M. D., Murshudov, G. N. and Papiz, M. Z. (2003) Macromolecular TLS refinement in REFMAC at moderate resolutions. Methods Enzymol. **374**, 300–321
39 Filip, C., Fletcher, G., Wulff, J. L. and Earhart, C. F. (1973) Solubilization of the cytoplasmic membrane of *Escherichia coli* by the ionic detergent sodium-lauryl sarcosinate. J. Bacteriol. **115**, 717–722
40 Kumar, S. S., Sankaran, K., Haigh, R., Williams, P. H. and Balakrishnan, A. (2001) Cytopathic effects of outer-membrane preparations of enteropathogenic *Escherichia coli* and co-expression of maltoporin with secretory virulence factor, EspB. J. Med. Microbiol. **50**, 602–612
41 Skillman, K. M., Barnard, T. J., Peterson, J. H., Ghirlando, R. and Bernstein, H. D. (2005) Efficient secretion of a folded protein domain by a monomeric bacterial autotransporter. Mol. Microbiol. **58**, 945–958
42 Hritonenko, V., Kostakioti, M. and Stathopoulos, C. (2006) Quaternary structure of a SPATE autotransporter protein. Mol. Membr. Biol. **23**, 466–474

43 von Heijne, G., Wickner, W. and Dalbey, R. E. (1988) The cytoplasmic domain of *Escherichia coli* leader peptidase is a "translocation poison" sequence. Proc. Natl. Acad. Sci. U.S.A. **85**, 3363–3366
44 Lehmann, S. and Harris, D. A. (1997) Blockade of glycosylation promotes acquisition of scrapie-like properties by the prion protein in cultured cells. J. Biol. Chem. **272**, 21479–21487
45 Kraulis, P. (1991) MOLSCRIPT: a program to produce both detailed and schematic plots of protein structures. J. Appl. Crystallogr. **24**, 946–950
46 Esnouf, R. M. (1997) An extensively modified version of MolScript that includes greatly enhanced coloring capabilities. J. Mol. Graphics Modell. **15**, 132–134
47 Goddard, T. D. (2007) Visualizing density maps with UCSF Chimera. J. Struct. Biol. **157**, 281–287
48 Rocchia, W., Alexov, E. and Honig, B. (2001) Extending the applicability of the nonlinear Poisson–Boltzmann equation: multiple dielectric constants and multivalent ions. J. Phys. Chem. B **105**, 6507–6514

Received 22 September 2010/7 February 2011; accepted 10 February 2011
Published as BJ Immediate Publication 10 February 2011, doi:10.1042/BJ20101548

Biochem. J. (2011) **435**, 577–587 (Printed in Great Britain) doi:10.1042/BJ20101548

online data

SUPPLEMENTARY ONLINE DATA

Autotransporter passenger domain secretion requires a hydrophobic cavity at the extracellular entrance of the β-domain pore

Yujia ZHAI*, Kai ZHANG*[1], Yanwu HUO*[1], Yanshi ZHU†, Qiangjun ZHOU*, Jiuwei LU*, Isobel BLACK†, Xiaoyun PANG*, Aleksander W. ROSZAK†, Xujia ZHANG*, Neil W. ISAACS† and Fei SUN*[2]

*National Laboratory of Biomacromolecules, Institute of Biophysics, Chinese Academy of Sciences, Beijing 100101, China, and †Department of Chemistry and WestChem, University of Glasgow, Glasgow G12 8QQ, U.K.

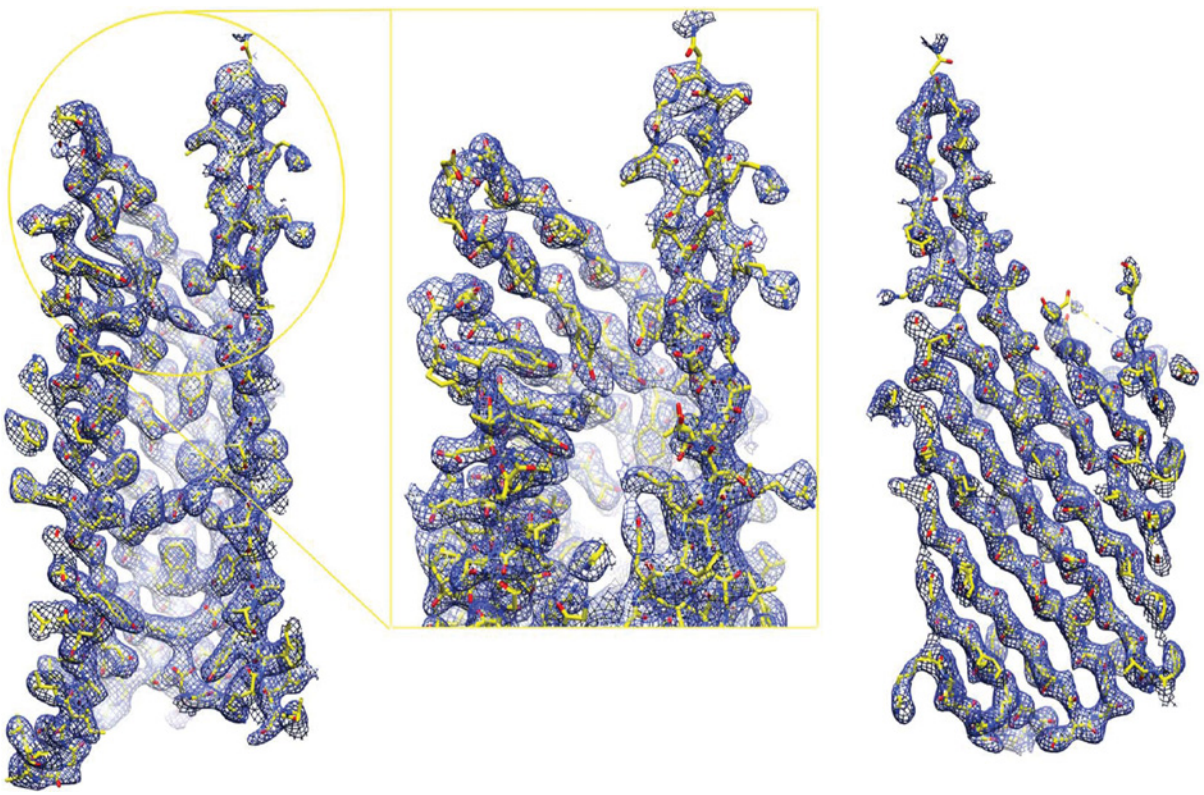

Figure S1 $2F_o - F_c$ electron-density appearance of BrkAβ contoured at 1.0σ

The $2F_o - F_c$ map is coloured blue and the structural model of BrkAβ is shown as sticks. On the left is the electron-density map of the β-barrel cross-section, in the middle is an enlarged view of the clear electron density around the extracellular region, and on the right is the electron-density map of the β-barrel. The Figure was made by using UCSF Chimera [1].

Immunolabelling electron microscopy

We used immunoelectron microscopy to investigate the localization of the expressed BrkA and its mutants in *E. coli*. The whole protocol is almost the same as reported previously [2]. Briefly, 2 ml of C41(DE3) cell suspension expressing BrkAΔ-PC or its mutants was harvested by centrifuging at 3500 ***g*** for 3 min and the supernatant was discarded. After washing with 40 mM phosphate buffer (pH 6.8), the pellet was fixed overnight in fixative buffer [8 % (w/v) paraformaldehyde, 80 mM potassium phosphate (pH 6.8), 0.75 M sorbitol and 0.2 % glutaraldehyde]. After washing again with phosphate buffer, the pellet was dehydrated in a gradient series of 30, 50, 70, 95 and 100 % ethanol (each 10–15 min) and infiltrated by 1:1 and 2:1 LR White™ (Electron Microscopy Sciences)/ethanol (each for 1 h) and finally by 100 % LR White™ overnight. After that, LR White™ was refreshed for a further 6 h of infiltration. All of the above processes were carried out at room temperature.

[1] These authors contributed equally to this work.
[2] To whom correspondence should be addressed (email feisun@ibp.ac.cn).
The crystal structure co-ordinates of BrkA β-domain were deposited in the PDB with accession number 3QQ2.

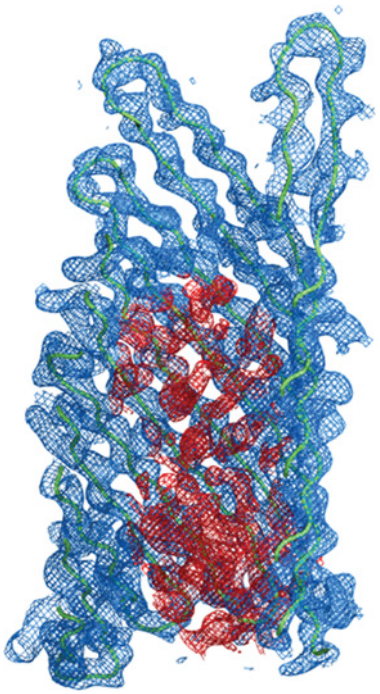

Figure S2 Electron-density map in the central pore of BrkAβ

The $F_o - F_c$ density map for untraced residues before Asp^{745} is coloured red and the $2F_o - F_c$ density map for the built residues after Asp^{745} is coloured blue. The Figure was made using PyMOL (http://www.pymol.org/).

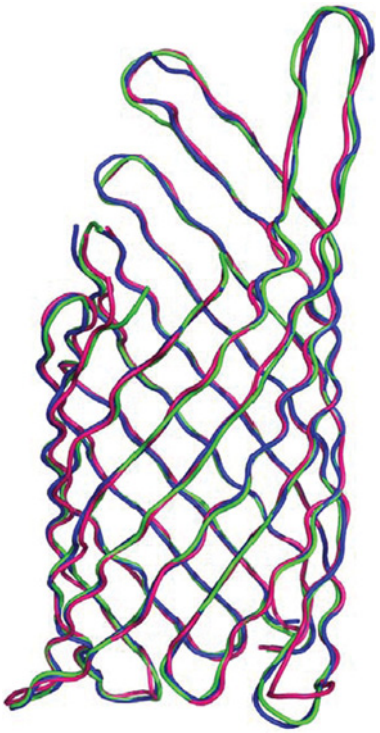

Figure S3 Superposition of the three molecules of BrkAβ in one asymmetric unit

The three molecules in one asymmetric unit, superposed using UCSF Chimera [1], are represented as ribbons and coloured red, blue and green. The Figure was produced using PyMOL (http://www.pymol.org/).

Finally, the resin was polymerized at 50 ± 1°C for 24 h. Ultrathin sections were made on an ultra-microtome (Leica UC6), and 70 nm sections were picked out and placed on to Formvar-coated copper grids for further immunolabelling.

The grids were washed four times with PBS, each for 2 min, and then were blocked with 5 % (v/v) NGS (normal goat serum) and 5 % (w/v) BSA in PBS for 30 min. Then the grids were applied overnight with mouse anti-His antibody (Sigma) at 4°C, which was diluted 1:100 in 5 % (w/v) BSA in PBS. The following steps were carried out at room temperature. After the grids were washed three times with 5 % (w/v) BSA in PBS, each for 10 min, they were treated for 1 h with goat anti-(mouse IgM) (μ-chain specific)–gold antibody (10 nm, Sigma) that was diluted 1:20 in 5 % (w/v) BSA in PBS. Then the grids were washed with four drops of PBS and six drops of double-distilled water. The sections were contrasted using 4 % aqueous uranyl acetate for 15 min and observed under transmission electron microscope (FEI Tecnai Spirit) operated at 80 kV.

To investigate further the significance of the membrane localization of expressed BrkAΔ-PC, we explored the stereology counting method that was used in our previous study [2] and also described by Mayhew et al. [3]. Briefly, 50 electron micrographs were selected randomly and a proper square lattice was superposed on to each micrograph. Then, the gold particles or the lattice intersecting points, located in the different regions (membrane, cytoplasm and whole micrograph), were counted and summarized respectively (see Supplementary Table S1). The LD (labelling density) in each region was calculated as number of observed gold particles (N_{obs})/number of counted intersecting points (P). The number of expected gold particles (N_{exp}) in each region was calculated as P times the LD of whole micrographs (LD_{total}). The RLI (relative labelling index) in each region was determined by $RLI = N_{obs}/N_{exp}$ and the χ^2 test by $\chi = (N_{obs} - N_{exp})^2/N_{exp}$. The counting results and the above parameters were calculated and are listed in Supplementary Table S1. Obviously, the RLI for gold on the membrane area is much larger than 1, indicating significant membrane localization propensity. The χ^2 test with χ much larger than 5.99 (in this test, the degree of system freedom, df, equals 2, as some gold particles are disperse outside cells) supports further the above conclusion. So it is significant that gold particles are mainly located on the membrane, i.e. most of the expressed BrkAΔ-PC were correctly targeted into the membrane.

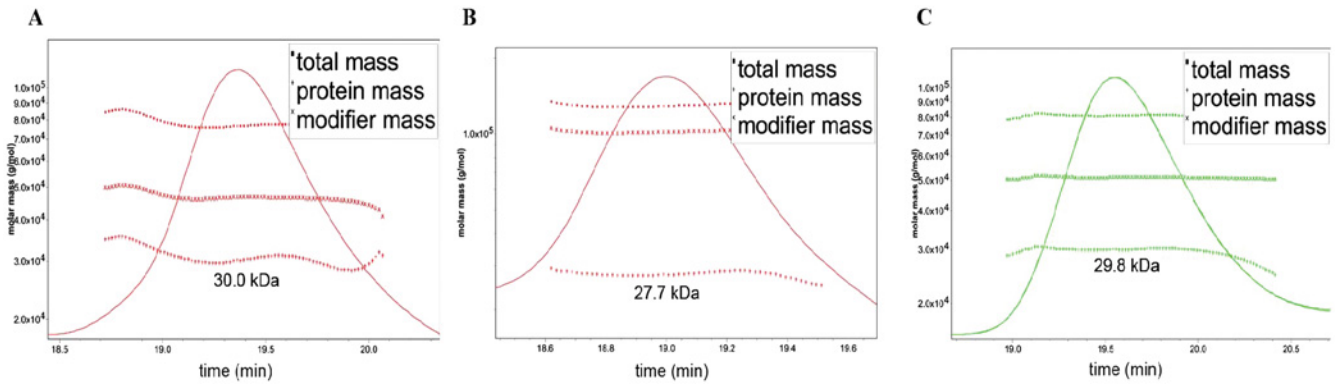

Figure S4 Profiles of SEC-MALS experiments on BrkAβ solubilized with different detergents

The *x*-axis represents the elution time and the *y*-axis represents the calculated molecular mass. The detergent used in each run was LDAO (**A**), dodecyl maltoside (**B**) or C_8E_4 (**C**). The elution peaks are shown as curves and the calculated molecular masses for total detergent–protein complex (total mass), BrkAβ alone (protein mass) and the pure detergent (modifier mass) are shown according to elution time in each profile.

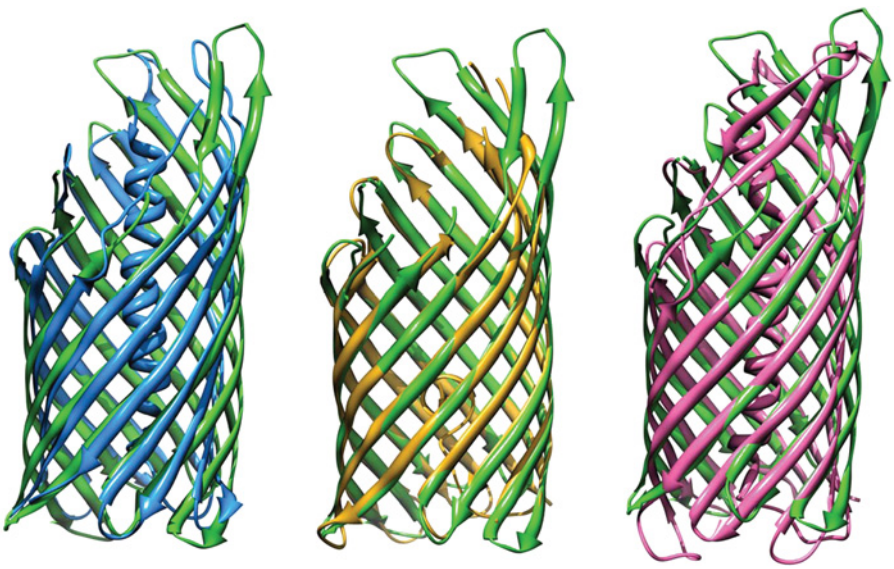

Figure S5 Comparison of BrkAβ with the β-domains of other ATs with known structures

Superpositions were performed using UCSF Chimera [1]. All of the structures are displayed as cartoons in PyMOL (http://www.pymol.org/). BrkAβ is coloured green, NalPβ is coloured blue, EspPβ is coloured gold, and EstAβ is coloured pink. The most distinctive region between BrkAβ and other AT β-domains is located around L4.

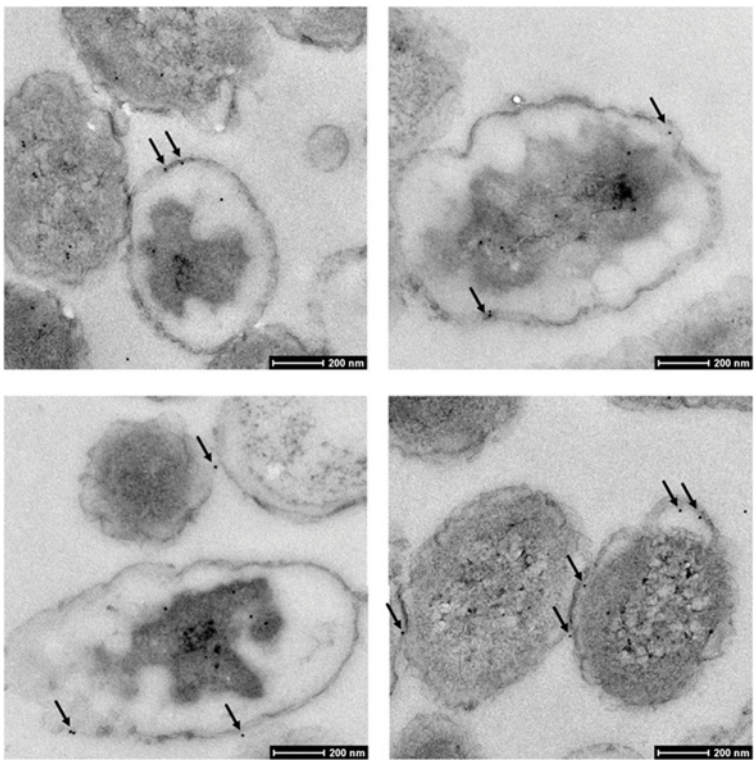

Figure S6 Immunolabelling electron microscopy of *E. coli* expressing BrkΔ-PC

Four selected electron micrographs of ultrathin sections of *E. coli* that express BrkAΔ-PC are given here. The thickness of each section is approximately 70 nm. Fixed *E. coli* exhibits clear membrane and plasma ultrastructure. Each section was immunolabelled using an anti-His antibody (Sigma) followed by a goat anti-(mouse IgM) (μ-chain specific)–gold antibody (Sigma). The nascent translated precursor of BrkAΔ-PC can be labelled in the plasma. The mature precursor of BrkAΔ-PC or its cleaved passenger can be identified by the nanogolds located on the membrane, which are indicated by black arrows. The diameter of colloid gold particles is approximately 10 nm and the scale bar represents 200 nm. For the detailed procedures of sample preparation and immunolabelling, see the Immunolabelling electron microscopy section of the Supplementary online data.

Table S1 Results of immunolabelling scored by stereology counting

For the terminology and explanation of each parameter, see the Immunolabelling electron microscopy section of the Supplementary online data and also [2]. When RLI>1 and χ^2 (df = 2, 0.05)>5.99, the localization conclusion is significantly obvious. *Counting colloidal gold particles or lattice points that are located around cell membrane area (acceptance zone: $\pm$ 15 nm). †Counting colloidal gold particles or lattice points that are located in the cytoplasm region. ‡Counting whole colloidal gold particles or lattice points that are found in each electron micrograph.

Count	Observed golds (N_{obs})	Observed intersecting points (P)	Labelling density (LD)	Expected golds (N_{exp})	RLI (N_{obs}/N_{exp})	χ^2
Membrane*	324	580	0.559	224	1.44	44.5
Cytoplasm†	1153	2519	0.458	968	1.19	35.4
Total‡	1567	4078				

REFERENCES

1 Goddard, T. D. (2007) Visualizing density maps with UCSF Chimera. J. Struct. Biol. **157**, 281–287
2 Zhou, Q. J., Sun, J., Zhai, Y. and Sun, F. (2010) Prokaryotic expression of active mitochondrial uncoupling protein 1. Prog. Biochem. Biophys. **37**, 56–62
3 Mayhew, T. M., Griffiths, G. and Lucocq, J. M. (2004) Applications of an efficient method for comparing immunogold labelling patterns in the same sets of compartments in different groups of cells. Histochem. Cell Biol. **122**, 171–177

Received 22 September 2010/7 February 2011; accepted 10 February 2011
Published as BJ Immediate Publication 10 February 2011, doi:10.1042/BJ20101548